Available online at www.sciencedirect.com
ScienceDirect
Journal of Sound and Vibration 321 (2009) 525–536
JOURNAL OF SOUND AND VIBRATION
www.elsevier.com/locate/jsvi

Aeroelastic analysis of rotor systems using trailing edge flaps

In-Gyu Lim[1], In Lee*

Korea Advanced Institute of Science and Technology, Daejeon 305-701, Republic of Korea

Received 29 February 2008; received in revised form 2 October 2008; accepted 24 October 2008
Handling Editor: L.G. Tham
Available online 1 January 2009

Abstract

An aeroelastic analysis of rotor blades with trailing edge flaps was conducted using large deflection-type beam theory for forward flight conditions with a focus on reducing vibration while minimizing control effort. The aerodynamic forces of the rotor blade were calculated using two-dimensional quasi-steady strip theory. For the analysis of forward flight, the nonlinear periodic blade steady response was obtained by integrating the full finite element equation in time through a coupled trim procedure with a vehicle trim. The objective function, which includes vibratory hub loads and active flap control inputs, was minimized by an optimal control process. Numerical simulations were performed for the steady-state forward flight of various advance ratios. Numerical results of the steady blade and flap deflections as well as the vibratory hub loads were also presented for various advance ratios and were compared with previously published analysis results obtained from modal analyses based on a moderate deflection-type beam theory.

1. Introduction

Vibration has great impact on helicopter performance and reliability and is an issue in helicopter design. Vibratory motion usually causes fatigue in structural components, reduces availability and increases the maintenance costs of helicopters. The need for vibration reduction is even more critical where passenger and crew comfort is concerned. The most significant source of vibration in a typical helicopter is the main rotor. The main rotor blades are subject to a highly unsteady aerodynamic environment arising from the airspeed differential between the advancing and retreating side of the rotor disk. The blades themselves are elastic, vibrating in response to the airloads and in turn the airloads are dependent on the blade elastic motions. Generally, studies on rotor blades have been performed for global deformation and cross-sectional analyses. One-dimensional global deformation analyses of rotor blades with consideration of geometrical nonlinearity have been classified into two types of beam theory: moderate deflection and large deflection. Most of the structural dynamic models for rotor blades are based on moderate deflection-type beam theories. These theories are based on ordering schemes and are valid for moderate deflections [1,2].

*Corresponding author at: Department of Aerospace Engineering, 373-1 Guseong-dong, Yuseong-gu, Republic of Korea. Tel.: +82 42 869 3717; fax: +82 42 869 3710.
E-mail address: inlee@kaist.ac.kr (I. Lee).
[1]Department of Aerospace Engineering, 371-1 Guseong-dong, Yuseong-gu, Republic of Korea.

0022-460X/$ - see front matter © 2008 Elsevier Ltd. All rights reserved.
doi:10.1016/j.jsv.2008.10.029

Nomenclature

A, **B**, **D**	effective sectional stiffness matrix
c_l	lift coefficient
c_{d0}	profile drag coefficient
C_T	thrust coefficient $(T/\rho_a \pi R^2 (\Omega R)^2)$
$\bar{e}_{11}, \bar{e}_{12}, \bar{e}_{13}$	strain vectors at reference point
q	generalized nodal displacement vector
α_s, ϕ_s	longitudinal and lateral shaft tilt angles, deg
θ_0, θ_{1c}, θ_{1s}	collective, lateral, longitudinal cyclic pitch angles, deg
$\kappa_1, \kappa_2, \kappa_3$	difference between undeformed and deformed strain curvature vectors
μ	advance ratio
σ	blade solidity $(N_b c/\pi R)$
ψ	azimuth angle, Ωt
$()_{,i}$	$\partial()/\partial x_i$, $i = 2,3$
$()'$	$\partial()/\partial x_1$
$(\dot{})$	$\partial()/\Omega\partial t = \partial()/\partial\psi$

A general purpose analysis, however, demands a large deflection model without any artificial restrictions on displacements or rotations due to the deformation and the degree of nonlinearity. Ordering schemes, although valuable tools in special purpose research, are not desirable for a general purpose approach. To overcome the limitations of previous models, structural models that are valid for large deflection and are not based on ordering schemes have been developed. There are no small angle approximations made and all kinematic nonlinear effects are included in the formulation of such models. To date, there have been relatively few studies on aeroelastic analysis of rotor blades using large deflection-type beam theories [3,4]. The blade airloads and aeroelastic response are essentially periodic in forward flight. The loads observed in the rotating system occur at multiple integer harmonics of the rotational speed. For a rotor with N_b identical blades, it is well known that the blade root shears and moments sum in such a manner that only pN_b/rev loads are transmitted to the fixed system, with p an arbitrary integer. The goal of most helicopter vibration reduction systems is the reduction of this N_b/rev motion. There are two different approaches for vibration reduction. One is to focus on a low vibration design process [5]. The other is to employ suppression devices. During the past several decades, active control of vibration has been investigated by many researchers. Active vibration control of the helicopter can be classified into two subcategories: the airframe-based control [6] and the rotor-based control. Among the various active rotor-based control approaches, higher harmonic control (HHC) is one such active method in which the swashplate is excited at the higher harmonics of the rotor rotational speed [7]. An alternative to HHC is individual blade control (IBC). IBC permits a wide range of excitation frequencies by placing the actuators directly into the rotating frame. Among the implementations of IBC, the active trailing edge flap (ATF) approach has received considerable attention due to its simplicity of implementation and the enhanced airworthiness it offers [8]. Milgram et al. presented a comprehensive study of vibration reduction in helicopters using an ATF [9]. The aeroelastic analysis in their study included a nonlinear aeroelastic rotor model, unsteady compressible aerodynamics of the flap and a multicyclic flap controller. The analytical results presented in their study were validated using experimental wind tunnel data. Straub and Charles investigated the dynamics and aerodynamics of rotors with trailing edge flaps using two different aeroelastic codes-CAMRAD/JA and CAMRAD II [10]. Shen and Chopra developed a comprehensive aeroelastic analysis of a fully coupled blade-flap-actuator system. The objective of the study was to investigate the effect of this coupling on vibration reduction with trailing edge flaps [11]. Zhang et al. looked at active-passive vibration reduction using trailing edge flaps and optimal blade structural properties [12]. Viswamurthy and Ganguli presented optimal locations of dual trailing-edge flaps to achieve minimum hub vibration levels in a helicopter, while incurring low penalty in terms of required trailing edge flap control power [13]. Kim et al. developed a resonant trailing edge flap actuation system (includes the piezoelectric actuator and the related mechanical and electrical elements for actuation) for helicopter rotors and evaluated experimentally [14].

In this paper, the finite element approach using large deflection-type beam theory is presented for the aeroelastic analysis of rotor blades with trailing edge flaps in forward flight. The aerodynamic forces are modeled using a two-dimensional quasi-steady strip theory considering the timesaving and reasonably good results although the results are inaccurate at quantitative point in comparison with those using

three-dimensional aerodynamic model. Nonlinear, periodic blade steady responses are obtained using time finite element method on a full finite element equation in the forward flight condition. Blade responses fully coupled with vehicle trim are solved to obtain the nonlinear blade response, pilot controls (θ_0, θ_{1c}, θ_{1s}) and vehicle attitude (α_s, ϕ_s). The effect of vibration reduction using trailing edge flaps is studied. The objective function, which includes vibratory hub loads and active flap control inputs, is minimized by an optimal control process. There is investigated how the nonlinear kinematic effects greatly affect the steady equilibrium and optimal trailing edge flap inputs using large deflection beam theory and full finite element analysis compared with the modal analysis using the moderate deflection beam theory and is shown that ATFs are effective and efficient for rotor vibration reduction.

2. Analysis

2.1. Structural dynamic model

A rotor blade rotating with angular velocity Ω is depicted in Fig. 1. Here, the triad $\mathbf{I}_1$, $\mathbf{I}_2$ and $\mathbf{I}_3$ is fixed in an inertia frame, the triad $\mathbf{i}_1$, $\mathbf{i}_2$ and $\mathbf{i}_3$ is fixed in a reference frame that rotates with respect to the inertia frame at a constant angular velocity $\Omega\mathbf{I}_3$. The triad $\mathbf{e}_1$, $\mathbf{e}_2$ and $\mathbf{e}_3$ is attached to a reference line along the axis of the undeformed blade and the triad $\mathbf{e}_1^*$, $\mathbf{e}_2^*$ and $\mathbf{e}_3^*$ is attached to a reference line along the axis of the deformed blade. The geometrical nonlinearities are described using coordinate transformation matrices with Euler angles in the present large deflection-type beam theory.

$$\mathbf{e}_i^* = \mathbf{t}_e(x_1)\mathbf{e}_i = \mathbf{T}(x_1)\mathbf{i}_i \quad \mathbf{T}(x_1) = \mathbf{t}_e(x_1)\mathbf{t}_g(x_1) \tag{1}$$

The transformation matrices $\mathbf{t}_g$, $\mathbf{t}_e$ and $\mathbf{T}$ are functions of the curvilinear axial coordinate x_1. Assuming that the initial curvatures are small and that the shearing strains are much smaller than unity in the Green–Lagrangian strain components, strain–displacement relations are represented as those in Ref. [15]. If higher order strain components and initial curvatures are neglected and general warping displacements are introduced in and out of plane of a cross-section, the strain–displacement relations can be expressed as follows [16]:

$$\begin{aligned}\varepsilon_{11} &= \bar{e}_{11} + x_3\kappa_2 - x_2\kappa_3 + w_1'\\ \gamma_{12} &= 2\bar{e}_{12} - x_3\kappa_1 + w_2' + w_{1,2}\\ \gamma_{13} &= 2\bar{e}_{13} + x_2\kappa_1 + w_3' + w_{1,3}\end{aligned}$$

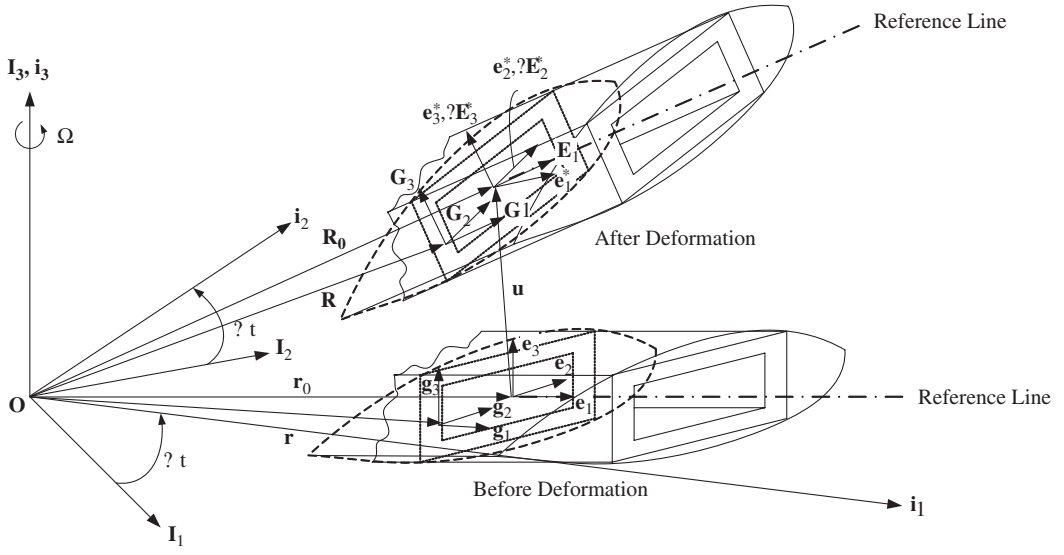

Fig. 1. Geometry and coordinate systems of a rotor blade before and after deformation.

$$\varepsilon_{22} = w_{2,2}$$
$$\gamma_{23} = w_{2,3} + w_{3,2}$$
$$\varepsilon_{33} = w_{3,3} \tag{2}$$

where x_1, x_2 and x_3 are curvilinear coordinates and w_1, w_2 and w_3 are the general warping displacements of an arbitrary point on the cross-section. The force strain $(\bar{e}_{11}, 2\bar{e}_{12}, 2\bar{e}_{13})$ and the moment strain $(\kappa_1, \kappa_2, \kappa_3)$ components are given in Ref. [16]. Here, $(.)'$ indicates the derivative with respect to x_1 and $(.)_{,i}$ denotes the derivatives with respect to x_i, $i = 2,3$.

The equations of motion for a rotor blade are obtained using Hamilton's weak principle

$$\int_{\psi_i}^{\psi_f} (\delta L + \delta W)\, \mathrm{d}\psi = \delta \mathbf{q}^{\mathrm{T}} \mathbf{p}\big|_{\psi_i}^{\psi_f} \tag{3}$$

where

$$L = T - U \quad \mathbf{p} = \frac{\partial L}{\partial \dot{\mathbf{q}}}$$
$$\delta U = \int_l \delta \begin{Bmatrix} \bar{\mathbf{e}} \\ \bar{\boldsymbol{\kappa}} \end{Bmatrix}^{\mathrm{T}} \begin{bmatrix} \mathbf{A} & \mathbf{B} \\ \mathbf{B}^{\mathbf{T}} & \mathbf{D} \end{bmatrix} \begin{Bmatrix} \bar{\mathbf{e}} \\ \bar{\boldsymbol{\kappa}} \end{Bmatrix} \mathrm{d}x_1$$
$$\delta T = \int_0^l \int_A \rho \{\delta \mathbf{V}\}^{\mathrm{T}} \{\mathbf{V}\}\, \mathrm{d}A\, \mathrm{d}x_1$$
$$\delta W = \int_0^l \int_A \delta \{R\}^{\mathrm{T}} \{f\}\, \mathrm{d}A\, \mathrm{d}x_1 \tag{4}$$

where δU, δT and δW are the variation of strain energy, the variation of kinetic energy and the virtual work of applied forces, respectively. $\bar{\mathbf{e}}$ and $\bar{\boldsymbol{\kappa}}$ vectors are defined as follows: $\bar{e} = \{\bar{e}_{11}\ \ 2\bar{e}_{12}\ \ 2\bar{e}_{13}\}^{\mathrm{T}}$, $\bar{\kappa} = \{\kappa_1\ \ \kappa_2\ \ \kappa_3\}^{\mathrm{T}}$ and the sectional stiffness matrices $\mathbf{A}$, $\mathbf{B}$ and $\mathbf{D}$ are 3×3 matrices that not only depend on the material properties but also cross-sectional geometry and the initial curvature and twists. In the case of isotropic material, these matrices are represented by the diagonal term, ρ is the mass density of the blade, V, the velocity with respect to the inertia frame ($\mathbf{V} = \dot{R} + \Omega I_3 \times R$) and f, the external force.

2.2. Aerodynamic model

In the present work, the aerodynamic lift and pitching moment acting on the blade were obtained by using a modification of Greenberg's extension [17] of Theodorsen's theory for a two-dimensional airfoil undergoing unsteady motion in an incompressible flow (Fig. 2). Considering a large aspect ratio wing in incompressible and inviscid flow, the wing/aileron combination undergoes two degrees of motion: plunge motion $h(t)$ and pitch motion $\varepsilon(t)$ about the blade elastic axis. The aerodynamically unbalanced trailing edge flap rotates about the flap hinge by the angle $\delta(t)$ relative to the chord line.

Two-dimensional quasi-steady strip theory was used to evaluate aerodynamic forces in forward flight. The components of resultant velocity $\mathbf{U}$ in the deformed blade coordinate system are given by

$$\begin{Bmatrix} U_R \\ U_T \\ U_P \end{Bmatrix} = \mathbf{T} \begin{Bmatrix} \dot{u}_1 - \Omega R_{02} - \Omega R \mu \cos\psi \\ \dot{u}_2 + \Omega R_{01} + \Omega R \mu \sin\psi \\ \dot{u}_3 + \Omega R \lambda_i \end{Bmatrix} \tag{5}$$

where $\dot{u}_i$ is the component of elastic velocity vector $\dot{\mathbf{u}}$ of blade and R_{0i}, the component of position vector $\mathbf{R}$ of an arbitrary point of the cross-section in the deformed blade configuration. R is the blade radius, Ω, the constant angular velocity, μ, the advance ratio, λ_i, the inflow ratio and ψ, the azimuth angle of the blade. The advance ratio μ and the inflow ratio λ_i are defined as nondimensionalized forward speed, $V/\Omega R$ and induced velocity, $v_{id}/\Omega R$, respectively. Drees linear inflow model was used for the rotor inflow distribution. The effects of compressibility and reversed flow were also included in the aerodynamic models.

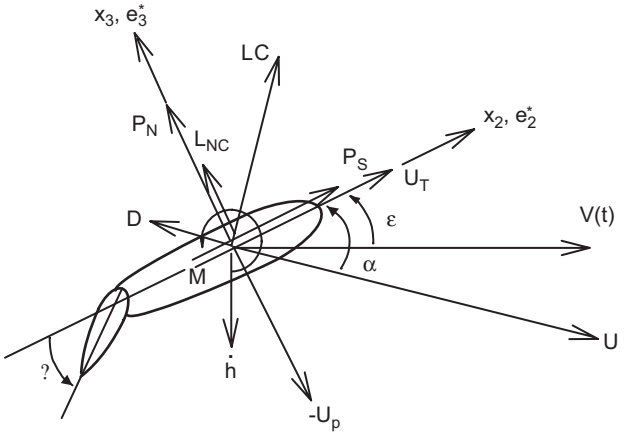

Fig. 2. Rotor blade airfoil section in general unsteady motion.

2.3. Blade steady response and coupled trim analysis

In this study, two-dimensional quasi-steady strip theory was used to evaluate aerodynamic forces in forward flight. For forward flight, the nonlinear, periodic steady response is obtained using a time finite element technique [18]. The virtual energy expression for the Hamilton's weak form can be obtained as follows:

$$\int_{\psi_i}^{\psi_f} \delta \mathbf{y}^{\mathrm{T}} \mathbf{l} \, \mathrm{d}\psi = \delta \mathbf{y}^{\mathrm{T}} \mathbf{b}|_{\psi_i}^{\psi_f} \tag{6}$$

where

$$\delta \mathbf{y} = \begin{Bmatrix} \delta \dot{\mathbf{q}} \\ \delta \mathbf{q} \end{Bmatrix} \quad \mathbf{l} = \begin{Bmatrix} \mathbf{L}_{\dot{q}} \\ \mathbf{L}_q + \mathbf{Q} \end{Bmatrix} \quad \mathbf{b} = \begin{Bmatrix} \mathbf{0} \\ \mathbf{p} \end{Bmatrix} \tag{7}$$

Here, $\mathbf{Q}$ represents the generalized forces and $\mathbf{L}$ denotes the Lagrangian of the system. $\mathbf{L}_{\dot{q}}$ and $\mathbf{L}_q$ are partial derivatives of $\mathbf{L}$ with respect to generalized coordinates $\dot{\mathbf{q}}$ and $\mathbf{q}$, respectively, which are composed of displacements and Euler angles, while $\mathbf{p} = \mathbf{L}_{\dot{q}}$ is the column vector of the generalized moment. ψ_i and ψ_f represent the initial and final states of nondimensionalized time, respectively. Using a first-order Taylor series expansion of the left-side of Eq. (6) with respect to a given state vector $\bar{\mathbf{y}}$, the following governing equation can be derived in an incremental form:

$$\int_{\psi_i}^{\psi_f} \delta \mathbf{y}^{\mathrm{T}} \bar{\mathbf{l}} \, \mathrm{d}\psi + \int_{\psi_i}^{\psi_f} \delta \mathbf{y}^{\mathrm{T}} \bar{\mathbf{K}} \Delta \mathbf{y} \, \mathrm{d}\psi = \delta \mathbf{y}^{\mathrm{T}} \mathbf{b}|_{\psi_i}^{\psi_f} \tag{8}$$

where the local tangent matrix $\bar{\mathbf{K}}$ is defined as

$$\bar{\mathbf{K}} = \begin{bmatrix} \mathbf{L}_{\dot{q}\dot{q}} & \mathbf{L}_{\dot{q}q} \\ \mathbf{L}_{q\dot{q}} + \mathbf{Q}_{\dot{q}} & \mathbf{L}_{qq} + \mathbf{Q}_q \end{bmatrix} \tag{9}$$

where $\mathbf{L}_{\dot{q}\dot{q}}$, $\mathbf{L}_{\dot{q}q}$, $\mathbf{L}_{qq}$, $\mathbf{Q}_{\dot{q}}$ and $\mathbf{Q}_q$ indicate the second and first derivatives with respect to the subscripts, respectively.

The propulsive vehicle trim analysis was fully coupled with previous blade steady response analysis to solve the blade response, pilot control inputs and vehicle orientation simultaneously. The vehicle trim solution was calculated from the overall nonlinear vehicle equilibrium equations: three force equations (vertical, longitudinal and lateral) and three moment equations (pitch, roll and yaw).

2.4. Control algorithm

In the present study, a single ATF located at 70% blade span location was used to introduce control input directly in the rotating reference frame (Fig. 3). In steady forward flight, the helicopter rotor system can be assumed to be periodic in time. This periodic nature of the system allows us to transform the control problem from the time domain to the frequency domain [19]. The control algorithm is based on the minimization of an objective function that is a quadratic function of hub vibratory loads and control input magnitudes. In this study, the control input is the flap deflection angle itself. The objective function for optimal control is given by Ref. [12]

$$J = Z_n^{\mathrm{T}} W_z Z_n + \delta_n^{\mathrm{T}} W_\delta \delta_n \tag{10}$$

where Z_n is the hub vibratory load vector containing N_b/rev sine and cosine harmonics. W_z and W_δ represent weights for the vibration and the control inputs, respectively. δ_n is the active flap control input vector containing cosine and sine higher harmonics, typically 3, 4, $5/rev$ or plus $2/rev$ harmonics for a four-bladed rotor. With this control input vector, the trailing edge flap deflection as a function of azimuth can be written as

$$\delta(\psi) = \sum_{i=2}^{5} [\delta_{ic} \cos(i\psi) + \delta_{is} \sin(i\psi)] \tag{11}$$

The optimal control input is obtained by the following optimality criteria:

$$\frac{\partial J}{\partial \delta_n} = 0 \tag{12}$$

The optimal control input δ_n can be solved from Eq. (12)

$$\delta_n = D(T_0^{\mathrm{T}} W_Z T_0)\delta_{n-1} - D(T_0^{\mathrm{T}} W_Z Z_{n-1}) \tag{13}$$

Define

$$D = (T_0^{\mathrm{T}} W_Z T_0 + W_\delta)^{-1}; \quad C = -DT_0^{\mathrm{T}} W_Z; \quad T_0 = \frac{\Delta Z_{n-1}}{\Delta \delta_{n-1}}$$

where T_0 is the transfer matrix numerically calculated by perturbing the control harmonics individually around the current control input using a forward difference method.

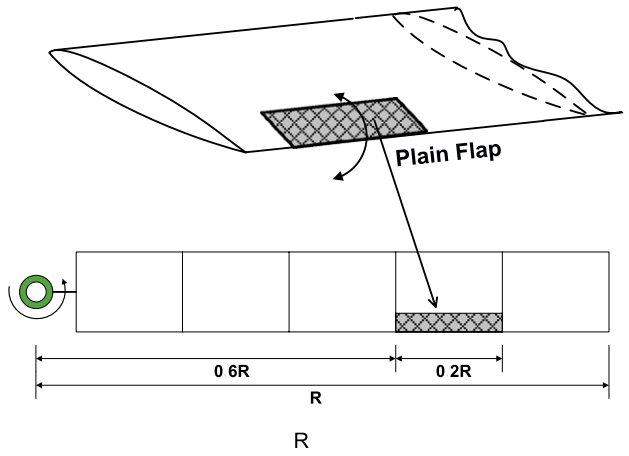

Fig. 3. Configuration of rotor blades with trailing edge flaps.

2.5. Numerical results

Aeroelastic analyses of rotor blades with trailing edge flaps were performed using the large deflection-type beam theory. Nonlinear periodic steady response was obtained by integrating the full finite element equations in time. Numerical results were obtained for a four-bladed, soft inplane, uniform hingeless rotor. The baseline vehicle and rotor blade properties are presented in Table 1. The trailing edge flap properties are presented in Table 2. A plain flap configuration was applied in this study (Fig. 3). It was assumed that the presence of flaps does not alter the mass distribution of rotor blades and that the stiffness changes of baseline blades are negligible. The blade was discretized into five four-noded cubic elements in the space domain and the time period of one rotor revolution was discretized into eight four-noded cubic elements in the time domain. The blade responses and vibratory hub loads were analyzed at two different advance ratios: the high advance ratio of 0.35 and the low advance ratio of 0.15. The present results obtained by the full finite element analysis in forward flight using the large deflection-type beam theory were compared with the previous published results obtained by a modal analysis using the moderate deflection-type beam theory. The present paper compares these two models to investigate the effect of vibration reduction using trailing edge flap and nonlinear kinematic effects due to large deflections. Fig. 4 shows nondimensional flap, torsion and lag tip deflections of the blade for one revolution at an advance ratio of $\mu = 0.15$. The present analysis was compared with the previous results given in Ref. [12] and a relatively good correlation between these two results about lag and

Table 1
Vehicle and rotor properties.

Number of blades	4
Radius, R (ft)	16.2
Hover tip speed (ft/s)	650
c/R	0.08
Solidity, σ	0.1
C_T/σ	0.07
Lock number, γ	6.34
Lift curve slope, a_0	5.73/rad
C_{d0}	0.0095
Blade mass per unit length, m_0 ($slug/ft$)	0.135
k_{m1}^2/R, k_{m2}^2/R	0.0001, 0.0004
Hub length, x_{hub}/R	0.04
Aerodynamic root cutout, x_{root}/R	0.10
Blade linear twist, θ_{tw}	-8.0°
Hub precone, β_{pc}	0.0
$EI_y/m_0\Omega^2R^4$	0.008345
$EI_z/m_0\Omega^2R^4$	0.023198
$GJ/m_0\Omega^2R^4$	0.00225
CG below hub (h/R)	0.2
Flat plat Area ($f/\pi R^2$)	0.01
Longitude and latitude offsets, $x_{c.g.}/R$, $y_{c.g.}/R$	0.0, 0.0

Table 2
Trailing edge flap parameters.

Flap chord ratio	c_f/c	0.20
Flap radius location along the blade		0.60–0.80
Flap mass per unit length	m_f/m_0	0.0844
Flap chordwise CG (after flap hinge)	r_I/c_f	0.149
Flap radius of gyration about flap hinge	r_{II}^2/c_f^2	0.109
Offset from blade elastic axis to flap hinge	d_f/c_f	0.55

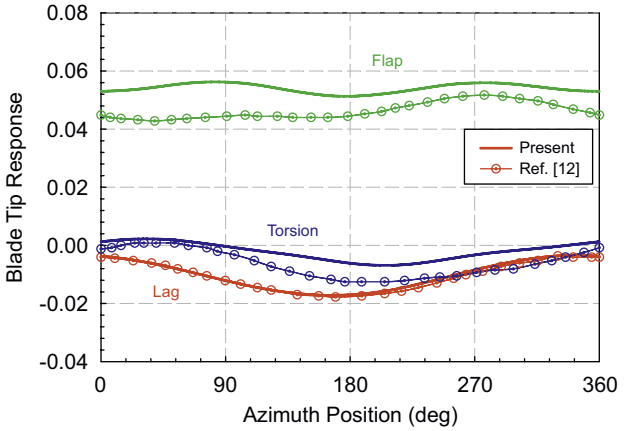

Fig. 4. Blade tip response without flap deflection ($\mu = 0.15$).

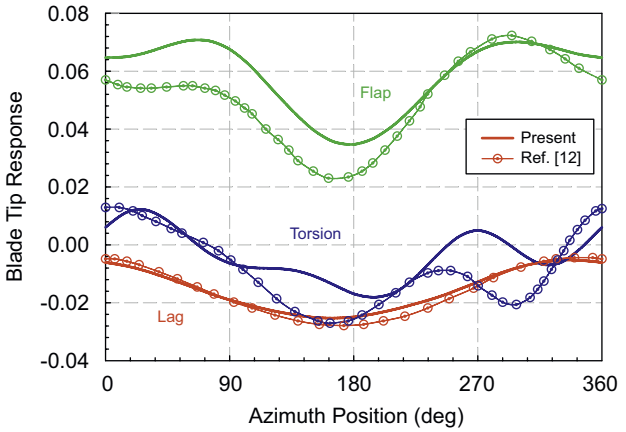

Fig. 5. Blade tip response without flap deflection ($\mu = 0.35$).

torsion deflections is shown in the Fig. 4. The results of Ref. [12] were obtained using modal analysis with a modal basis of eight coupled rotating natural modes (three flap, three lag and two torsion modes). Fig. 5 shows the blade tip response at an advance ratio of $\mu = 0.35$. There are differences between the results of the two models and these differences increase as the forward speed increases due to the nonlinear kinematic effects that manifest as the scale increases. The nonlinear kinematic effects greatly affect the torsion steady response as the forward speed increases. Figs. 6 and 7 show pilot control inputs and vehicle orientation at advance ratios $\mu = 0.15$ and 0.35, respectively. A relatively good correlation between these two results is shown in Figs. 6 and 7. The $4/rev$ vibratory hub loads (longitudinal force: F_x, lateral force: F_y, vertical force: F_z, rolling moment: M_x, pitching moment: M_y and yawing moment: M_z for the hub nonrotating fixed frame) are shown at $\mu = 0.15$ in Fig. 8. As shown in Fig. 8, the trends between two results are quite similar, though some differences appear in magnitude. The flap was actuated in 2, 3, 4 and $5/rev$ sine and cosine harmonics to reduce the vibratory hub loads. The corresponding active flap deflections at advance ratios $\mu = 0.15$ and 0.35 are shown in Figs. 9 and 10. It was observed that $2/rev$ active flap inputs were the largest among the four input harmonics. Fig. 11 shows the simultaneously reduced $4/rev$ vibratory hub loads along with the baseline vibratory hub loads at an advance ratio of $\mu = 0.15$. The vibratory hub loads were reduced by 25–90% from the baseline vibration level. Fig. 12 shows the simultaneously reduced $4/rev$ vibratory hub loads along with the baseline vibratory hub loads at an advance ratio of $\mu = 0.35$. The present analysis was compared with the previous results given in [12]. The vibratory hub loads were reduced by 70–96% from the baseline vibration level and a similar reduction trend between two results was observed.

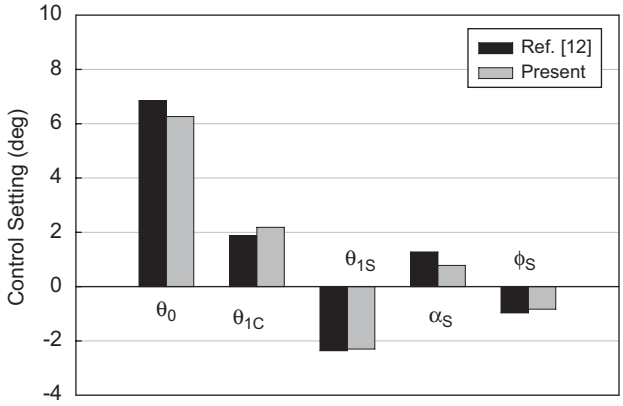

Fig. 6. Trim control setting without flap deflection ($\mu = 0.15$).

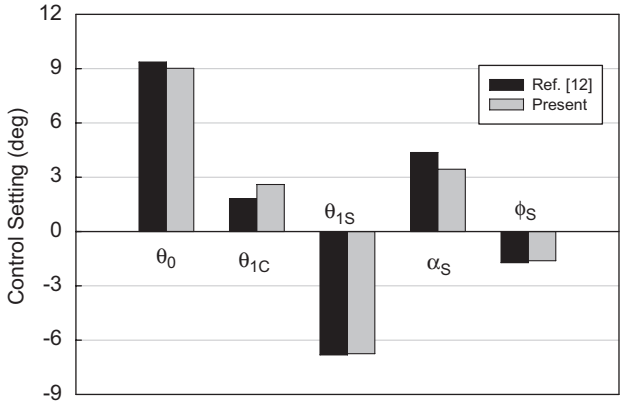

Fig. 7. Trim control setting without flap deflection ($\mu = 0.35$).

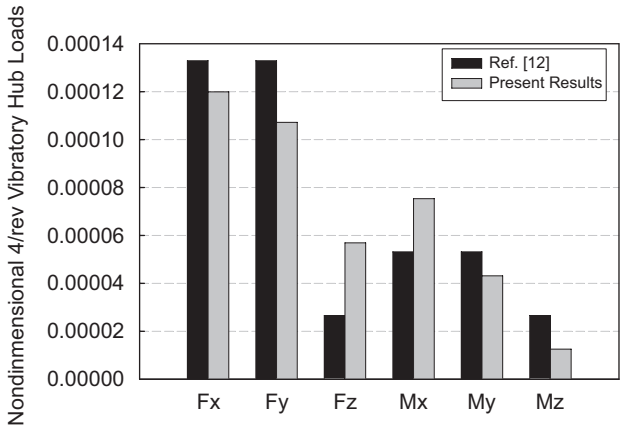

Fig. 8. The 4/*rev* vibratory hub loads without flap deflection ($\mu = 0.15$).

3. Conclusions

In this paper, an aeroelastic analysis of rotor blades with trailing edge flaps in forward flight was presented. A finite element analysis was conducted using the large deflection beam model. Nonlinear, periodic blade

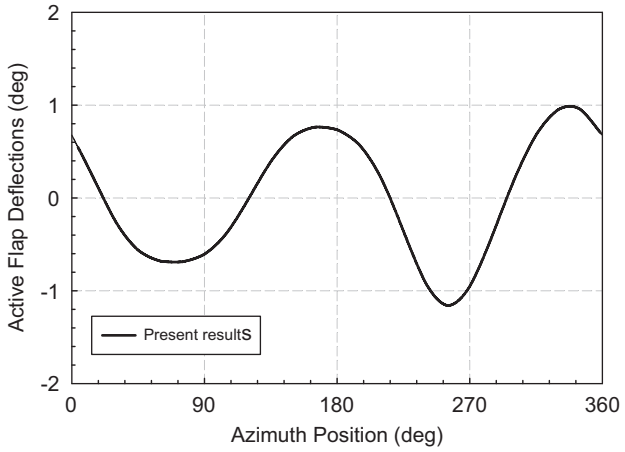

Fig. 9. Flap deflection for retrofit design ($\mu = 0.15$).

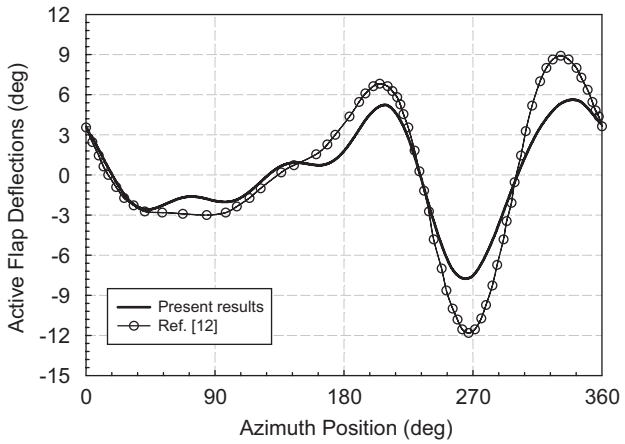

Fig. 10. Flap deflection for retrofit design ($\mu = 0.35$).

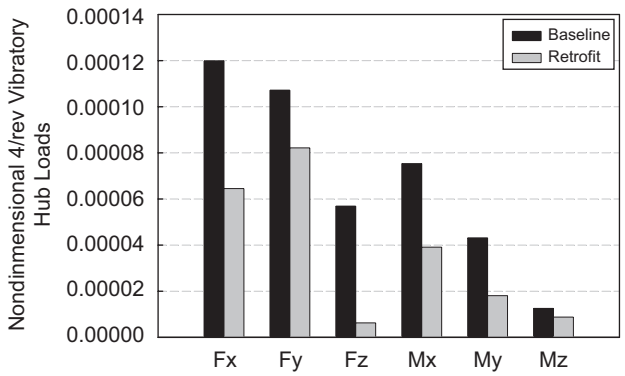

Fig. 11. The 4/*rev* vibratory hub loads for retrofit design ($\mu = 0.15$).

steady response was computed using the time finite element method on full finite element equation with full coupling of the propulsive vehicle trim. The periodic steady tip deflections and vibratory hub loads for rotor blades with and without active flap control were compared with those obtained by a modal approach using the

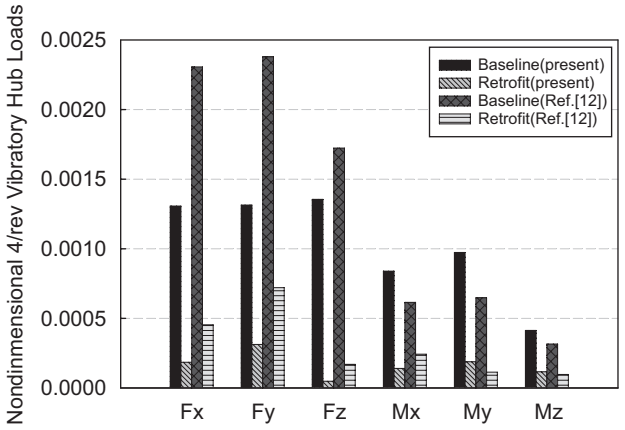

Fig. 12. The 4/*rev* vibratory hub loads for retrofit design ($\mu = 0.35$).

moderate deflection-type beam theory. The results show that nonlinear kinematic effects greatly affect the steady response and vibratory hub loads as the forward speed increases and that ATFs are effective and efficient for rotor vibration reduction.

Acknowledgment

This research has been supported by BK21 (the Brain Korea 21 Project).

References

[1] A. Rosen, P.P. Friedmann, The nonlinear behavior of elastic slender straight beams undergoing small strains and moderate rotations, *ASME Journal of Applied Mechanics* 46 (1) (1979) 161–168.
[2] D.H. Hodges, E.H. Dowell, Nonlinear equations of motion for elastic bending and torsion of twisted non-uniform rotor blades, NASA TN D-7818, 1974.
[3] S.M. Jeon, I. Lee, Aeroelastic response and stability analysis of composite rotor blades in forward flight, *Composites: Part B* 32 (2001) 249–257.
[4] I.G. Lim, I. Lee, Aeroelastic analysis of bearingless rotors using large deflection beam theory, *AIAA Journal* 45 (3) (2007) 599–606.
[5] P.P. Friedmann, Helicopter vibration reduction using structural optimization with aeroelastic/multidisciplinary constraints—a survey, *Journal of Aircraft* 28 (1) (1991) 8–21.
[6] J.T. Pearson, R.M. Goodall, I. Lyndon, Active control of helicopter vibration, *Computing & Control Engineering Journal* 5 (6) (1994) 277–284.
[7] K. Nguyen, I. Chopra, Application of higher harmonic control to rotor operating at high speed and thrust, *Journal of the American Helicopter Society* 35 (3) (1990) 78–89.
[8] S.R. Viswamurthy, R. Ganguli, Effect of piezoelectric hysteresis on helicopter vibration control using trailing edge flaps, *Journal of Guidance Control and Dynamics* 29 (5) (2006) 1201–1209.
[9] J.H. Milgram, I. Chopra, F. Straub, Rotor with trailing edge flaps: analysis and comparison with experimental data, *Journal of the American Helicopter Society* 43 (4) (1998) 319–332.
[10] F.K. Straub, B.D. Charles, Aeroelastic analysis of rotors with trailing edge flaps using comprehensive codes, *Journal of the American Helicopter Society* 46 (3) (2001) 192–199.
[11] J. Shen, I. Chopra, Aeroelastic stability of trailing-edge flap helicopter rotors, *Journal of the American Helicopter Society* 48 (4) (2003) 236–243.
[12] J. Zhang, Active-passive Hybrid Optimization of Rotor Blades with Trailing Edge Flaps, Ph.D. Dissertation, Department of Aerospace Engineering, The Pennsylvania State University, 2001.
[13] S.R. Viswamurthy, R. Ganguli, Optimal placement of trailing-edge flaps for helicopter vibration reduction using response surface methods, *Engineering Optimization* 39 (2) (2007) 185–202.
[14] J.-S. Kim, K.W. Wang, E.C. Smith, Development of a resonant trailing-edge flap actuation system for helicopter rotor vibration control, *Smart Materials & Structures* 16 (6) (2007) 2275–2285.

[15] A.D. Stemple, S.W. Lee, Large deflection static and dynamic finite element analysis of composite beams with arbitrary cross sectional warping, *Proceedings of the AIAA/ASME/ASCE/AHS/ACS 30th Structures, Structural Dynamics and Materials Conference*, AIAA Paper 89-1363, Washington, DC, 1989, pp. 1788–1798.
[16] M.H. Cho, I. Lee, Aeroelastic stability of hingeless rotor blade in hover using large deflection theory, *AIAA Journal* 32 (7) (1994) 1472–1477.
[17] J.M. Greenberg, Airfoil in Sinusoidal Motion in a Pulsating Stream, 1947, NACA TN-1326.
[18] M. Borri, Helicopter rotor dynamics by finite element time approximations, *Computers & Mathematics with Applications* 12A (1) (1986) 149–160.
[19] W. Johnson, Self-tuning regulators for multicyclic control of helicopter vibration, NASA TP-1996, 1982.